Capillary evaporation in pores

2006 J. Phys.: Condens. Matter 18 6517

(http://iopscience.iop.org/0953-8984/18/28/007)

INSTITUTE OF PHYSICS PUBLISHING JOURNAL OF PHYSICS: CONDENSED MATTER

J. Phys.: Condens. Matter **18** (2006) 6517–6530 doi:10.1088/0953-8984/18/28/007

Capillary evaporation in pores

R Roth and K M Kroll

Max-Planck Institut für Metallforschung, Heisenbergstraße 3, D-70589 Stuttgart, Germany
and
Institut für Theoretische und Angewandte Physik, Universität Stuttgart, Pfaffenwaldring 57, D-70569 Stuttgart, Germany

E-mail: Roland.Roth@mf.mpg.de

Received 13 April 2006, in final form 1 June 2006
Published 28 June 2006
Online at stacks.iop.org/JPhysCM/18/6517

Abstract

We combine a density functional theory (DFT) treatment of capillary evaporation in a cylindrical pore with the morphometric approach in order to study the formation and breaking of bubbles in a hydrophobically lined part of a cone. The morphometric approach, in which the grand potential of a system is described in four geometrical terms with corresponding thermodynamical coefficients, allows extrapolation or scaling from macroscopic system sizes to nanoscales. Since only a small number of fluid particles are involved in bubble formation, it is a pseudo phase transition, and the system is subjected to fluctuations between states with and without a bubble. Fluctuations are not included in a DFT treatment, which makes it possible to explore both states of the system in great detail, in contrast to computer simulations, in which averages might be obscured by fluctuations.

1. Introduction

The physics of confined fluids has been studied in great detail both experimentally [1–7] and theoretically [8–12]. Several phenomena are known to be produced by the confining geometry. For example, one finds that a fluid that is in the gas phase in bulk, i.e. without confinement, can condense into a liquid phase at a much higher density if confined by hydrophilic walls, despite the fact that this liquid would not be stable in the bulk. This phenomenon is called capillary condensation and can be observed in experiments measuring adsorption isotherms of gases in porous media. A closely related phenomenon is the transition of a fluid, in its stable bulk liquid phase, confined by hydrophobic walls, into a gas phase at much smaller number density, which would not be stable without the confining geometry. This transition is called capillary evaporation, or 'bubble formation' in more colourful language. Both transitions show hysteresis loops [13] in experiments,which are typical signs for first-order phase transitions.

Most of the experimental and theoretical effort was targeted at understanding these transitions in the case of fluids close to saturation. Theoretical studies often employed a simple

slit geometry of two parallel planar walls. Under these conditions, the transition can take place at a moderate level of confinement so that mesoscopic arguments based on thermodynamics have proven very helpful.

Recent studies indicate that a phenomenon similar to capillary evaporation might be important in the physics of ion channels [14–23]. Ion channels are proteins in cell membranes that allow the passive transport of ions along their electro-chemical gradient [24]. The main function of these proteins is to control the transport of ions through the membrane by opening and closing the channel, a process called gating, and in some cases by allowing only specific ions to pass through the pore, a phenomenon called selectivity. Our work is inspired by the wish to improve the understanding of the role of bubble formation and breaking in the gating mechanism of ion channels.

To this end, we start in section 2 by recalling the basics of capillary evaporation in simple geometries using a thermodynamics point of view. Then in section 3 we show microscopic density functional theory (DFT) calculations [25] of a square-well fluid inside an infinitely long hydrophobically lined cylinder. In our DFT calculations, we focus on the density profile $\rho(r)$ and the corresponding grand potential Ω of a fluid as a function of the cylinder radius R_{cyl}, while capillary evaporation takes place. The insight gained from these DFT calculations we transfer to and exploit in our morphometric approach [26, 27], presented in section 4. In morphometry, the free energy of a liquid confined in a pore is expressed by four terms that describe the geometry of the pore and the corresponding thermodynamic coefficients. This separation of geometry and thermodynamics allows us to extrapolate or scale the behaviour of the system from macroscopic sizes down to small sizes in the nanometre regime and below. Furthermore, the morphometric approach makes calculations very efficient, so that the formation of a bubble in the gate due to a change in geometry can be studied in detail. The bubble formation in the geometry we consider constitutes a pseudo phase transition, in which a finite number of particles is involved. This makes the system close to the transition point unstable, in the sense that thermal fluctuation can cause the formation or breaking of the bubble and the system can constantly change state. This varying behaviour makes bubble formation hard to study reproduceably and hence convincingly in computer simulations. We conclude with an outlook in section 5.

2. Capillary evaporation in simple geometries

We consider a square-well fluid in the grand canonical ensemble and describe its structure and thermodynamic properties within the framework of DFT. The inter-particle interaction potential is given by

$$V_{\mathrm{sw}}(r) = \begin{cases} \infty & r < 2R_{\mathrm{HS}}, \\ -\varepsilon & 2R_{\mathrm{HS}} \leqslant r < R_{\mathrm{sw}}, \\ 0 & \text{otherwise}, \end{cases} \tag{1}$$

where R_{HS} and R_{sw} is the hard-sphere and the square-well radius, respectively, and ε is the square-well depth. The functional $\Omega[\rho(\mathbf{r})]$ of the grand potential has the form [25]

$$\Omega[\rho(\mathbf{r})] = \mathcal{F}[\rho(\mathbf{r})] + \int \mathrm{d}^3 r\, \rho(\mathbf{r})(V_{\mathrm{ext}}(\mathbf{r}) - \mu). \tag{2}$$

The intrinsic Helmholtz free energy functional $\mathcal{F}[\rho(\mathbf{r})] = \mathcal{F}_{\mathrm{id}}[\rho(\mathbf{r})] + \mathcal{F}_{\mathrm{ex}}[\rho(\mathbf{r})]$ can be split into an exactly known ideal gas contribution $\mathcal{F}_{\mathrm{id}}[\rho(\mathbf{r})]$ and an approximate excess (over the ideal gas) free energy functional $\mathcal{F}_{\mathrm{ex}}[\rho(\mathbf{r})] = \mathcal{F}_{\mathrm{ex}}^{\mathrm{HS}}[\rho(\mathbf{r})] + \mathcal{F}_{\mathrm{ex}}^{\mathrm{sw}}[\rho(\mathbf{r})]$. $V_{\mathrm{ext}}(\mathbf{r})$ denotes the

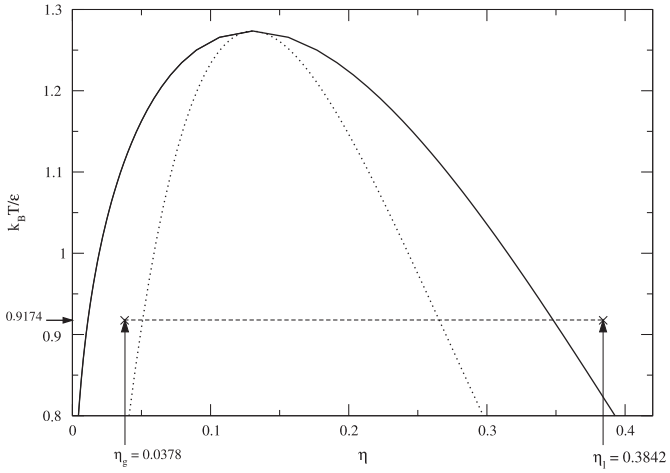

Figure 1. The fluid-gas binodal of a square-well fluid with $R_{sw} = 3R_{HS}$ as a function of reduced temperature k_BT/ε and the fluid packing fraction $\eta = \rho 4\pi R_{HS}^3/3$. In our DFT calculation, we consider the reduced temperature $k_BT/\varepsilon = 0.9174$ and a liquid (l) packing fraction of $\eta_l = 0.3842$. We find that a gas (g) with $\eta_g = 0.0378$ has the same chemical potential as the corresponding liquid.

external and μ the chemical potential of the fluid. $\mathcal{F}_{ex}[\rho(\mathbf{r})]$ can be further split into a hard-sphere reference part $\mathcal{F}_{ex}^{HS}[\rho(\mathbf{r})]$, for which we employ the White Bear version [29, 30] of fundamental measure theory [31], and a square-well part

$$\mathcal{F}_{ex}^{sw}[\rho(\mathbf{r})] = \tfrac{1}{2}\int \mathrm{d}^3r' \int \mathrm{d}^3r''\rho(\mathbf{r}')\rho(\mathbf{r}'')V_{attr}(|\mathbf{r}' - \mathbf{r}''|), \tag{3}$$

with a simple mean-field approximation for the inter-particle attraction $V_{attr}(r)$, which is $-\varepsilon$ for $r < R_{sw}$ and zero otherwise. Except for the external potential $V_{ext}(\mathbf{r})$, which plays an important role in the present study of confined fluids, the system is fully specified.

Before considering confined fluids, we recall the bulk phase behaviour of the square-well fluid. Since we are interested in fluid behaviour, we assume that the density profile $\rho(\mathbf{r})$ reduces to the constant bulk density ρ. From the bulk grand potential $\Omega_{bulk} = \Omega[\rho(\mathbf{r}) = \rho]$, we calculate the bulk pressure $p(\rho) = -\Omega_{bulk}/V$, where V is the volume, and the chemical potential $\mu(\rho) = \partial f/\partial\rho$, with the free energy density $f = F/V$. Two fluid phases, denoted by I and II, with corresponding number densities ρ_I and ρ_{II}, coexist if they are in mechanical and chemical equilibrium, i.e. if

$$p(\rho_I) = p(\rho_{II}), \qquad \text{and} \qquad \mu(\rho_I) = \mu(\rho_{II}). \tag{4}$$

For a square-well radius $R_{sw} = 3R_{HS}$ we obtain the fluid phase diagram shown in figure 1. Below the critical temperature, the fluid phase can separate into a liquid phase with a high bulk density and a gas phase with a low bulk density. Note that the mean-field perturbation theory, equation (3), predicts a phase diagram that is not sensitive to the detailed choice of parameters ε and R_{sw}. It rather predicts phase diagrams that can be rescaled onto a 'master phase diagram'. One finds, using the Carnahan–Starling equation of state for the hard-sphere contribution, that the critical point is located at $\eta_c \approx 0.1304$ and $k_BT_c/\varepsilon \approx 0.0472(R_{sw}/R_{HS})^3$.

If we bring a square-well liquid into contact with a single purely repulsive planar wall, the fluid develops, in general, an inhomogeneous density profile $\rho(z)$, where z denotes the distance from the wall. $\rho(z)$ can be calculated by minimizing the DFT [25] with an appropriate external wall potential that accounts for the interaction between the liquid and a hydrophobically lined

pore. For a liquid state very close to the coexisting density $\rho_{\rm II}(T)$, one can observe complete drying [32] and a growth of a macroscopically thick gas film at the wall as the density ρ approaches the coexisting liquid density $\rho_{\rm II}$ at a given temperature T, or as the deviation $\delta\mu = \mu - \mu_{\rm co}(T)$ of the chemical potential from its value at coexistence $\mu_{\rm co}(T)$ approaches zero.

In the present study, however, we shall stay away from these state points, as indicated in the phase digram in figure 1 by the state with reduced temperature $k_{\rm B}T/\varepsilon = 0.9174$ and packing fraction $\eta = 4\pi R_{\rm HS}^3\,\rho/3 = 0.3842$.

In order to quantify the change in the grand potential due to the inhomogeneous structure $\rho(z)$ close to the wall, we define σ, the planar wall surface tension, as

$$\sigma = \frac{1}{A}(\Omega[\rho(z)] + pV), \tag{5}$$

by subtracting the bulk term $-pV$ from the total grand potential of the system $\Omega = \Omega[\rho(z)]$. A is the surface area of the wall. In the thermodynamical limit, $V \to \infty$, the grand potential Ω and A also go to infinity. However, σ is an intrinsic quantity and remains finite. Note that the value of σ depends on the definition of the dividing surface [33], which in turn defines the volume V. However, the value of $\Omega = -pV + \sigma A$ remains the same for all definitions.

For a state point significantly far away from the binodal, as chosen in the present case, the interaction of the liquid and a single hydrophobic wall is not sufficient to destabilize the high-density liquid in favour of a low-density gas. The pressure in the liquid phase away from coexistence is always higher than in a gas phase at the same chemical potential, so that the surface contribution to the grand potential cannot compete with the volume term. For the gas phase to be more stable than the liquid phase, its grand potential $\Omega_{\rm g} = -p_{\rm g}V + \sigma_{\rm g}A$ must be more negative than the grand potential of the liquid phase $\Omega_{\rm l} = -p_{\rm l}V + \sigma_{\rm l}A$, with $V = AL$ and $A, L \to \infty$ in the thermodynamic limit. This cannot be accomplished, since even the smallest difference in the pressure would make the difference of the volume terms, $(-p_{\rm l} + p_{\rm g})AL$, arbitrarily larger than the difference in the surface terms, $(\sigma_{\rm l} - \sigma_{\rm g})A$.

When we add a second, parallel, wall at distance L, the behaviour of the system changes *qualitatively*. We consider the situation of two identical walls for simplicity. Note that the value of L also depends on the definition of the dividing surface, i.e. it measures the distance between the parallel dividing surfaces of the opposing walls. If L is large compared to the bulk correlation length ξ of the liquid, the grand potential of the system in the slit geometry can be written as [11]

$$\Omega_i^{\rm slit} \approx -p_i V + 2\sigma_i A, \qquad i = l, g, \tag{6}$$

where we have used that the walls are independent and the surface tensions σ_i are those of a single wall. Since the volume term is now scaled by a finite length L, it is possible that the liquid phase is destabilized in a slit geometry for sufficiently small plate separations. For phase equilibrium between a liquid phase and a gas phase with densities $\rho_{\rm l}$ and $\rho_{\rm g}$, respectively, at a wall separation $L_{\rm CE}$ it is necessary that their grand potentials and their chemical potentials are equal, which can be expressed, after dividing $\Omega_i^{\rm slit}$ by the area A, as

$$-p_{\rm l}L_{\rm CE} + 2\sigma_{\rm l} = -p_{\rm g}L_{\rm CE} + 2\sigma_{\rm g}, \qquad \text{and} \qquad \mu(\rho_{\rm l}) = \mu(\rho_{\rm g}). \tag{7}$$

This equilibrium condition can be solved to determine the slit width

$$L_{\rm CE} = \frac{2\Delta\sigma}{\Delta p}, \tag{8}$$

at which the capillary evaporation (CE) transition takes place. Clearly, since $\Delta p \equiv (p_{\rm g} - p_{\rm l})$ is negative, equation (8) has a physical solution only if $\Delta\sigma \equiv (\sigma_{\rm g} - \sigma_{\rm l})$ is also negative,

which holds true for hydrophobic walls. Equation (7) or (8) describe a competition between the volume and the surface contributions to the grand potential of the two fluid phases.

For a slit width $L > L_{\mathrm{CE}}$, the volume term in the grand potential dominates and stabilizes the liquid phase, whereas for $L < L_{\mathrm{CE}}$ the surface term in the grand potential becomes more important and the slit favours the gas phase. Note that a gas that is stabilized in the slit pore has the same chemical potential as the liquid phase and would be meta-stable in the bulk, i.e. would lie between the binodal (full line) and spinodal (dotted line) at $\eta_{\mathrm{g}} = 0.0378$—see figure 1.

Before we switch to a more complicated geometry, it is very instructive to consider the phenomena of capillary evaporation in an infinitely long cylindrical pore. The (approximate) form of the grand potential in the slit pore, equation (6), is well known and tested, at least for state points close to saturation, against microscopic theories, but the case of a cylindrical pore seems less understood.

Following the morphometric approach, we propose that the grand potential in contact with a complex-shaped wall can be written as [26, 27]

$$\Omega_i \approx -p_i V + \sigma_i A + \kappa_i C + \bar{\kappa}_i X, \tag{9}$$

where V and A are, as before, the volume and surface area defined by the dividing interface. The corresponding thermodynamic coefficients are $-p_i$ and σ_i, the negative of the pressure and the *planar* wall surface tension in phase i, respectively. Two additional geometrical measures are required in order to take the effects of curvature of the dividing interface into account, namely

$$C \equiv \int_{\partial V} H \,\mathrm{d}A, \qquad \text{and,} \qquad X \equiv \int_{\partial V} K \,\mathrm{d}A \tag{10}$$

the integrated (over the surface area A) mean and Gaussian curvatures $H = (1/R_{\mathrm{I}} + 1/R_{\mathrm{II}})/2$ and $K = 1/(R_{\mathrm{I}} R_{\mathrm{II}})$, respectively. R_{I} and R_{II} are the two principal radii of curvature, which are sufficient to describe any type of local curvature in three dimensions, if the surface is smooth. The radii of curvature are positive if the curvature is convex and negative in the case of concave curvature. The corresponding thermodynamic coefficients are the bending rigidities κ_i and $\bar{\kappa}_i$. The bending rigidities account for a change in the grand potential due to the curvature of the wall–fluid interface and the corresponding inhomogeneous structure in the fluid.

The morphometric form of the grand potential has been suggested to describe the thermodynamics of a fluid in contact with *convex* walls. However, away from a critical point or a wetting or drying transition, the morphometric form of the grand potential should provide a good description also for a fluid inside a pore, if the size of the pore is sufficiently large compared to the correlation length ξ. We will comment on this point when we present our DFT results in the next section.

For an infinitely long cylinder with radius R, the geometrical measures are readily calculated, and we obtain $V = R^2 \pi L$, $A = 2\pi RL$ and $C = -\pi L$. Note that the integrated mean curvature C is negative, because we are considering the *inside* of the cylinder, where the curvature is concave and the radius of curvature is negative. The fourth measure X vanishes, because the Gaussian curvature K of a cylinder is zero. Hence the morphometric form of the grand potential of a fluid inside a cylinder is given by,

$$\Omega_i^{\mathrm{cyl}} \approx -p_i R^2 \pi L + \sigma_i 2\pi RL - \kappa_i \pi L, \tag{11}$$

and we take the length of the cylinder $L \to \infty$. Note that, although the coefficient κ_i has the dimension of a line tension, its physical meaning is very different. It describes, as mentioned before, the change in grand potential of the liquid or the gas due to the curved wall. Using the morphometric form for $\Omega_i^{\mathrm{cyl}}/(\pi L)$, we can formulate the equilibrium condition between a liquid phase and a gas phase inside the cylindrical pore:

$$-p_{\mathrm{l}} R_{\mathrm{CE}}^2 + 2\sigma_{\mathrm{l}} R_{\mathrm{CE}} - \kappa_{\mathrm{l}} = -p_{\mathrm{g}} R_{\mathrm{CE}}^2 + 2\sigma_{\mathrm{g}} R_{\mathrm{CE}} - \kappa_{\mathrm{g}}, \qquad \text{and} \qquad \mu(\rho_{\mathrm{l}}) = \mu(\rho_{\mathrm{g}}). \tag{12}$$

The radius R_{CE} at which capillary evaporation takes place can be expressed explicitly in terms of the thermodynamic coefficients as

$$R_{\mathrm{CE}} = \frac{\Delta\sigma - \sqrt{(\Delta\sigma)^2 - \Delta p \Delta\kappa}}{\Delta p}, \tag{13}$$

where we have introduced, in addition to Δp and $\Delta\sigma$ defined earlier, the difference in the bending rigidities in the gas phase and the liquid phase, $\Delta\kappa \equiv (\kappa_{\mathrm{g}} - \kappa_{\mathrm{l}})$. It would be possible to proceed with a spherical cavity, however the expression for the radius at which capillary evaporation takes place is rather lengthy and provides no additional insight.

The thermodynamic arguments used in this section remain valid even if long-ranged interactions, such as dispersion forces, are considered, as long as one stays away from critical points and from the complete wetting or complete drying regime close to the binodal. In the complete wetting or complete drying regime, additional fluctuation-induced corrections to the Kelvin equation are required [28]. Since we consider only state points sufficiently far away from the binodal, these problems do not occur in our study.

3. DFT treatment of capillary evaporation in cylindrical pores

In order to verify the validity of the morphometric approach for the description of capillary evaporation inside infinitely long cylindrical pores, we perform DFT calculations. We have to choose an external potential $V_{\mathrm{ext}}(r)$ that defines the cylindrical pore. Since we wish to make a connection to the gating process in ion channels, we follow the approach from [34] and use a hard-sphere fluid of a given high density ($\eta_{\mathrm{w}} = 0.4$, $R_{\mathrm{w}} = 0.825 R_{\mathrm{HS}}$) which is kept outside the pore region by a hard-wall potential. The square-well fluid inside the pore can hardly penetrate into the region which is occupied by the wall fluid. The wall fluid thereby exerts an effective external potential $V_{\mathrm{ext}}(r)$ on the fluid inside the pore. We have calculated the external potential $V_{\mathrm{ext}}(r)$ so that it leads to the same density profile $\rho(r)$ of the square-well fluid inside the pore as the wall fluid does. $V_{\mathrm{ext}}(r)$ therefore corresponds to an atomically rough hydrophobic protein wall, which is averaged over the symmetry angle and the z-axes.

We perform a series of DFT calculation of a square-well fluid inside a cylindrical pore with radius R_{cyl}. We fix the reduced temperature $k_{\mathrm{B}}T/\varepsilon = 0.9174$ and the chemical potential so that it corresponds to a *bulk* packing fraction of the fluid $\eta = 0.3842$. The fluid density corresponds to a bulk concentration of 55.5M, the concentration of water at normal condition, if we assume that the hard-sphere radius $R_{\mathrm{HS}} = 1.4$ Å. This state point is considerably far from the binodal, so that one can expect that a capillary evaporation transition will take place at rather small values of $R_{\mathrm{cyl}}/R_{\mathrm{HS}}$.

In figure 2 we show the equilibrium density profiles $\rho(r)$ for varying values of R_{cyl}. Note that, by enforcing cylindrical symmetry in the density profile, which simplifies the calculations considerably, we restrict the results either to a liquid- or a gas-like density profile. For $R_{\mathrm{cyl}} \geqslant 6R_{\mathrm{HS}}$, we find that the liquid phase is stable in the cylindrical pore. In that case, we observe a high density of the square-well fluid in the centre of the pore and a continuous, smooth decrease to zero close to the wall $r \to R_{\mathrm{cyl}}$. For $R_{\mathrm{cyl}} \leqslant 5R_{\mathrm{HS}}$, the liquid phase inside the pore is not stable and we find a gas phase at low density. The gas packing fraction, which is indicated in the phase diagram in figure 1, is $\eta_{\mathrm{g}} = 0.0378$ and follows from the equilibrium condition that the gas phase with this density has the same chemical potential as the high-density liquid.

To ensure that the system undergoes a capillary evaporation transition and to locate the radius R_{CE} at which it takes place, we also determine $\Omega[\rho(r)]/L$, the grand potential (per unit length) corresponding to the density profiles. We show the results as symbols in figure 3.

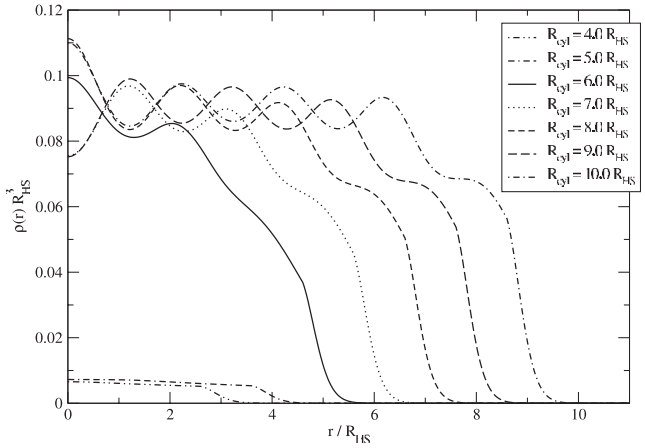

Figure 2. Density profiles, $\rho(r)$, of a square-well fluid inside a cylindrical pore with hydrophobic wall–particle interaction as a function of the radius R_{cyl}. For radii $R_{\mathrm{cyl}} \geqslant 6R_{\mathrm{HS}}$ we find a liquid in the pore, while for $R_{\mathrm{cyl}} \leqslant 5R_{\mathrm{HS}}$ we find a gas. However, note that, due to hysteresis effects, it is not possible to determine the location of the capillary evaporation transition, which takes place at $R_{\mathrm{cyl}} = R_{\mathrm{CE}} \approx 5.99R_{\mathrm{HS}}$, from the density profiles alone.

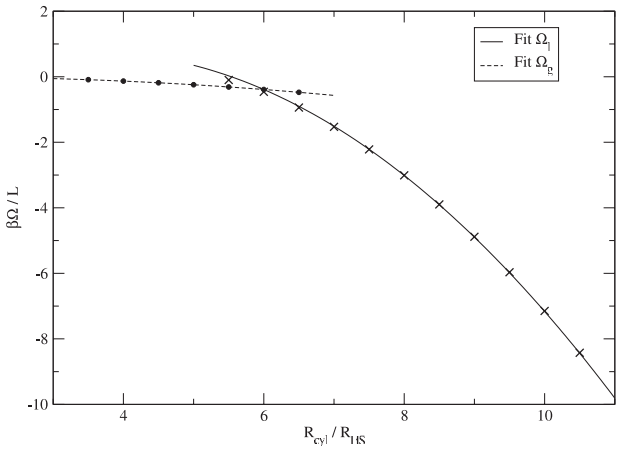

Figure 3. The grand potential per unit length of a square-well fluid inside an infinitely long cylindrical pore as function of the radius R_{cyl}. For large values of R_{cyl} we find the liquid branch, and for small values of R_{cyl} we find the gas branch of the grand potential. Symbols correspond to DFT results and the full and dashed lines denote least-square fits according to the morphometric form, equation (11), of a fluid inside a cylindrical pore. The agreement between the morphometric form and the numerical data is excellent, confirming the validity of morphometry in this situation.

There are several interesting features to appreciate. Obviously, there are two separate branches of the grand potential: one corresponding to the liquid phase for large values of R_{cyl} and the other corresponding to the gas phase for small values of R_{cyl}. This, together with the density profiles shown in figure 2, demonstrates that a capillary evaporation transition happens—it is not sufficient to look solely at the profiles. It is a strength of DFT that we are able to study both the profiles and the grand potentials at the same time, thereby elucidating the behaviour of the system.

Table 1. Thermodynamic coefficients p_i, σ_i and κ_i, $i = l, g$, obtained for a liquid and a gas inside a cylindrical pore from a fit to DFT results, assuming a morphometric form for the grand potential, equation (11).

	Liquid	Gas
η_i	0.3842	0.0378
$\beta p_i R_{\mathrm{HS}}^3$	6.077×10^{-2}	5.507×10^{-3}
$\beta \sigma_i R_{\mathrm{HS}}^2$	2.166×10^{-1}	7.128×10^{-3}
$\beta \kappa_i R_{\mathrm{HS}}$	5.360×10^{-1}	1.122×10^{-2}

We can employ our DFT results, shown as symbols in figure 3, to verify the validity of the morphometric approach for the present problem. According to morphometry, the grand potential, equation (11), is quadratic in the radius of the cylinder. Using the thermodynamic coefficients p_i, σ_i and κ_i as fitting parameters, we fit equation (11) to our DFT data. The full and dashed lines in figure 3 are the results of the fits to the grand potentials of the liquid and gas branches, respectively. The lines are in excellent agreement with the numerical data (symbols). The high quality of the fits demonstrates that the morphometric form of Ω can be used, despite the fact that the pore is rather narrow, i.e. the pore size is sufficiently large compared to the correlation length ξ. This finding allows the conclusion that, for the problem considered here, one can separate the thermodynamic coefficients from the geometry of the pore. Furthermore, we have verified that, within small numerical error bars, we find the *same* thermodynamical coefficients also in a spherical geometry, as we should, if the morphometric form is valid.

The thermodynamic coefficients as obtained by the fits summarized in table 1. The pressures p_i, $i = l, g$, are bulk properties and therefore can also be determined from the bulk equation of state. Both results for p_i are in good agreement. Using these coefficients and equation (13), we obtain $R_{\mathrm{CE}} = 5.99 R_{\mathrm{HS}}$ as the cylinder radius at which the transition takes place.

4. Capillary evaporation in a complex geometry

For simple geometries, such as a slit pore or an infinitely long cylindrical pore, it is straightforward to perform DFT calculations in order to study the capillary evaporation phenomenon. It is also most instructive to study the thermodynamics and the density profiles at the same time. For more complex geometries, a 'brute-force' [35] approach, in which density profiles are obtained by minimizing the DFT for the full geometry, is much more challenging. Therefore, in the following we will use only the morphometric approach to study the analogue of capillary evaporation in a complex geometry. The geometrical model that we wish to study is inspired by the structure of the voltage-gated potassium ion channels [36, 37], shown in a simplified model geometry in figure 4, which we approximate by part of a cone. The parameters that prescribe the geometry are the radii R_1 and R_2 and the height H. In our model, R_1 and H are kept fixed and R_2 varies from a value large enough to stabilize the liquid in the gate to a value small enough to allow for a closed gate with a gas bubble of height h—see figure 4. We consider both ends of the cone (or gate) to be big reservoirs of liquid, which will prevent the bubble from growing to macroscopic sizes. The bottom part of the gate connects to a spherical cavity of the potassium channel, while the top part of the gate connects to the inside of the cell. Due to the geometrical constraints, the bubble, if it forms, will always have a finite size, and a finite number of liquid particles will be involved in the evaporation process. Hence, the formation of a bubble represents a pseudo phase transition. This implies that the state of the

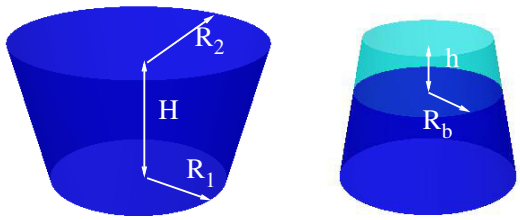

Figure 4. The model geometry of the gate of a potassium ion channel. The radius R_1 and the height H are fixed and the radius R_2 is allowed to vary from a large value, for the open state of the gate, to a smaller value, for the closed state. In the open state the whole gate is filled with liquid, while in the closed state a gas bubble of height h closes the gate and thereby stops the permeation of ions through the channel. R_b is the radius of the bubble at the bottom. Note that, in the closed state, there are two liquid–gas interfaces at the top and bottom of the bubble.

(This figure is in colour only in the electronic version)

system can fluctuate between an open state and a closed state, and the probability of a transition is determined by the Boltzmann factor of the difference in grand potentials between the states. In contrast to the capillary evaporation process in the infinitely long cylinder, which was either completely filled by the liquid or by the gas, we will observe two liquid–gas interfaces at the top and bottom ends of the bubble.

In the following, we consider the gate with a fixed configuration, i.e. with a given radius R_2, in a state in which it is entirely filled with the liquid and in a state with a bubble of height h. By comparing these two states, we examine the possibility of bubble formation in the gate and study the behaviour of the bubble, once it has formed. We employ the morphometric form of the grand potential for both a filled gate, which we denote as the open (op) state, and a gate with a gas bubble, which we denote as the closed (cl) state.

The grand potential of the open state is given by

$$\Omega^{\mathrm{op}}_{\mathrm{gate}}(R_2) = -p_l\, V(H, R_1, R_2) + \sigma_l\, M(H, R_1, R_2) + \kappa_l\, C(H, R_1, R_2), \tag{14}$$

with the thermodynamical coefficients p_l, σ_l and κ_l as specified in table 1. The geometrical measures for part of a cone with height $\tilde{h}$ and radii r_1 and r_2 at the bottom and the top, respectively, are specified by the volume

$$V(\tilde{h}, r_1, r_2) = \frac{\pi \tilde{h}}{3}\left(r_1^2 + r_2^2 + r_1 r_2\right), \tag{15}$$

the surface area of the cone shell

$$M(\tilde{h}, r_1, r_2) = \pi(r_1 + r_2)\sqrt{\tilde{h}^2 + (r_1 - r_2)^2}, \tag{16}$$

and the integrated mean curvature (over the cone shell area inside the cone)

$$C(\tilde{h}, r_1, r_2) = -\pi \tilde{h}. \tag{17}$$

As in the case of an infinitely long cylinder, the integrated Gaussian curvature (over the cone shell area) vanishes in the cone geometry, so that the grand potential of the liquid-filled gate in the morphometric form, equation (14), is fully specified by three terms.

The morphometric form of a closed state of the gate, with a bubble of height h, is more complicated and contains terms for the part of the gate filled by the liquid, terms for the part filled by the gas, and terms due to the presence of the liquid–gas interfaces. Assuming the simple geometry shown in figure 4, we can write as an ansatz

$$\Omega^{\mathrm{cl}}_{\mathrm{gate}}(h, R_2) = -p_{\mathrm{l}}\, V(H-h, R_1, R_{\mathrm{b}}) + \sigma_{\mathrm{l}}\, M(H-h, R_1, R_{\mathrm{b}}) + \kappa_{\mathrm{l}}\, C(H-h, R_1, R_{\mathrm{b}}) - p_{\mathrm{g}}\, V(h, R_{\mathrm{b}}, R_2) + \sigma_{\mathrm{g}}\, M(h, R_{\mathrm{b}}, R_2) + \kappa_{\mathrm{g}}\, C(h, R_{\mathrm{b}}, R_2) + \sigma_{\mathrm{lg}}\, (A(R_{\mathrm{b}}) + A(R_2))\,. \tag{18}$$

Note that, by employing this ansatz, we reduce the complexity of the problem of finding the state with the lowest grand potential from a full DFT calculation in a complex geometry to a parametric minimization problem with a single free parameter, namely the bubble height h. The detailed shape of the bubble corresponding to the lowest grand potential will differ slightly from the shape assumed by this ansatz, however we expect that *all* the essential physics is included in our approach. Furthermore, the simplicity of our approach allows us to gain deep insight into the driving factors of bubble formation and breaking in a gate-like geometry.

The radius R_{b} in equation (18) depends on the geometrical parameters of the cone R_1, R_2, H and the bubble height h via $R_{\mathrm{b}} = R_2 + h(R_1 - R_2)/H$. Clearly, $R_2 < R_1$ is required to make this relation meaningful in the present context. Note that additional line-tension terms of the form $\tau L_{3\mathrm{p}}$ arise where the liquid–gas interface meets the wall, and a three phase (3p) contact line of length $L_{3\mathrm{p}}$ is created. However, these contributions are expected to be small and should change the results, discussed below, only slightly. Furthermore, the calculation of τ is tedious and would require a brute-force DFT calculation. Therefore we neglect the line-tension terms in the following. Again, we want to emphasize that this line-tension term is not to be confused with the curvature term which is proportional to κ_i, $i = l, g$.

In order to fully specify the grand potential, equation (18), we require an additional thermodynamic coefficient, namely σ_{lg}, the liquid–gas interface tension. Unfortunately, this quantity is rather difficult to calculate, since we have to consider the interface between a liquid at high density and a gas phase, which is stabilized only in the confined geometry. This calculation could only be performed in a brute-force application of DFT, which is prohibitive. Therefore we approximate the value of σ_{lg} by the liquid–gas surface tension of the free interface between unconfined coexisting liquid and gas phases at the same temperature. This quantity can be calculated easily, and we obtain $\beta\sigma_{\mathrm{lg}} R^2_{\mathrm{HS}} = 8.549 \times 10^{-2}$. Note, however, that the thermodynamic coefficients listed in table 1 correspond to the stable liquid at $\eta_{\mathrm{l}} = 0.3842$ and the meta-stable (in the bulk) gas at $\eta_{\mathrm{g}} = 0.0378$, as indicated in the table.

The surface area of the liquid–gas interface also calls for attention, since the radii R_1, R_2 and R_{b} are measured at the dividing interface. The meaning of these radii becomes apparent when the density profiles in figure 2 are inspected carefully. For a cylindrical pore radius of, for example, $R_{\mathrm{cyl}} = 10R_{\mathrm{HS}}$, the liquid density profile drops to a vanishing density at $r \gtrsim 9R_{\mathrm{HS}}$. Therefore we use

$$A(r) = \pi(r - R_{\mathrm{HS}})^2 \tag{19}$$

as the surface area of the liquid gas interface.

The first question to be addressed concerns the most probable bubble height h_0. This can be rephrased by asking which value of h maximizes the difference in the grand potential between a closed and a open state of the gate, i.e.

$$\frac{\partial}{\partial h}\left(\Omega^{\mathrm{cl}}_{\mathrm{gate}}(h, R_2) - \Omega^{\mathrm{op}}_{\mathrm{gate}}(R_2)\right)\Big|_{h=h_0} = 0. \tag{20}$$

This equation can be solved explicitly. The result for $h_0(R_2)$, however, is quite lengthy and we therefore only show numerical results. With this result, we can answer the question for which range of R_2 the stable state of the gate is the closed one. We denote the maximal value of R_2 for which a closed gate is stable with $R_2^{\max}$, which is defined through

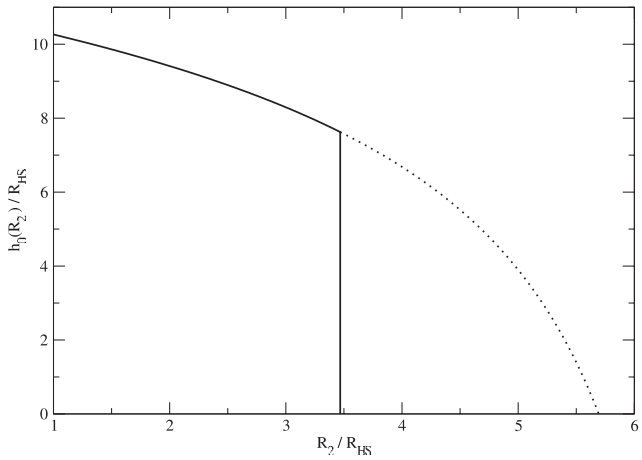

Figure 5. The most probable height $h_0(R_2)$ of the gas bubble as a function of R_2. Due to the competition between the various contributions of the grand potential, the bubble height at the transition point at $R_2 = R_2^{\max}$ is non-vanishing. For $R_2 < R_2^{\max}$, a bubble with height $h_0(R_2)$ is the stable state, indicated by the full line, and the gate is closed. For $R_2 > R_2^{\max}$, the closed gate is meta-stable, which is denoted by the dotted line—see figure 6.

$$\Delta\Omega(R_2 = R_2^{\max}) \equiv \Omega_{\text{gate}}^{\text{cl}}(h_0, R_2^{\max}) - \Omega_{\text{gate}}^{\text{op}}(R_2^{\max}) = 0, \tag{21}$$

which can be calculated numerically.

In order to quantify our results, we have to specify the geometry of the gate considered. We choose $R_1 = 7.14R_{\text{HS}}$ and $H = 14.29R_{\text{HS}}$, which corresponds to $R_1 \approx 10$ Å and $H \approx 20$ Å if we assign R_{HS} a value of 1.4 Å, as would be appropriate for water. For this choice of parameters, we plot in figure 5 the most probable bubble height h_0 as a function of the parameter R_2. For large values of R_2, we find that a bubble of height $h_0(R_2)$ would be meta-stable, which we indicate by the dotted line. In this regime, the most stable state of the gate is the open state. As R_2 reaches the value of $R_2^{\max}$, the bubble height jumps to a non-vanishing value, and if R_2 is further decreased the bubble height increases slightly, as shown by the full line in figure 5. For the present model, we find that the pseudo transition, at which a bubble forms in the gate, takes place for $R_2^{\max} \approx 3.46R_{\text{HS}} \approx 4.84$ Å, as follows from the difference in grand potentials of a closed state and an open state of the gate as a function of R_2—see figure 6.

The value of $h_0(R_2^{\max})$ at the transition point can be readily understood. When we compare the grand potential for the closed state to that of the open state, by calculating $\Delta\Omega$ we find

$$\begin{aligned}\Delta\Omega(R_2) = &-\Delta p V(h, R_{\text{b}}, R_2) + \Delta\sigma M(h, R_{\text{b}}, R_2) + \Delta\kappa C(h, R_{\text{b}}, R_2) \\ &+ \sigma_{\text{lg}}\left(A(R_{\text{b}}) + A(R_2)\right),\end{aligned} \tag{22}$$

with Δp, $\Delta\sigma$, and $\Delta\kappa$ defined above. In order to have the gate closed, we require $\Delta\Omega < 0$, which we can analyse by comparing the different contributions to $\Delta\Omega$. For the situation that we consider here, we find that three terms in equation (22) are positive: $-\Delta p V(h, R_{\text{b}}, R_2) > 0$, describing the fact that the volume term prefers the stable bulk phase in the gate, which is the liquid, $\Delta\kappa C(h, R_{\text{b}}, R_2) > 0$, and $\sigma_{\text{lg}}(A(R_{\text{b}}) + A(R_2)) > 0$, which simply states the fact that the formation of two liquid–gas interfaces costs energy. These three contributions to $\Delta\Omega$ have to be balanced by the only negative term, $\Delta\sigma M(h, R_{\text{b}}, R_2) < 0$. However, this balance can only be established if the surface area of the cone shell M is sufficiently large, which requires a height $h_0(R_2^{\max}) > 0$.

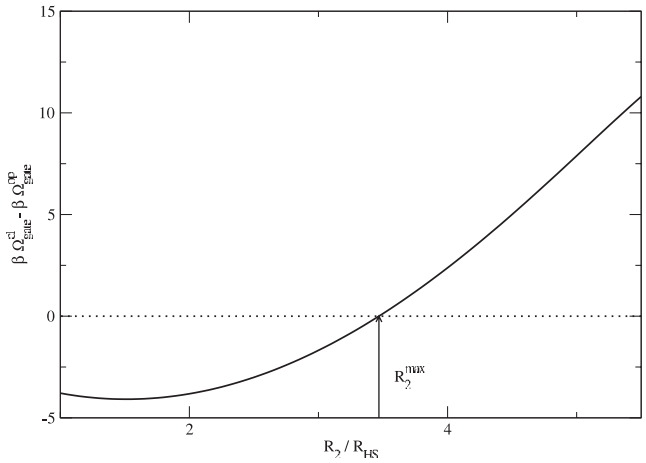

Figure 6. The difference in grand potentials between a closed state and an open state of the gate as a function of R_2. If this difference is positive, the open state is stable, otherwise the closed state is stable. For $R_2 = R_2^{\max}$, the difference in grand potentials vanishes and thereby marks the transition point between the states of the gate.

Within this model of the gate, it is easy to estimate the energy required to *control* the state of the gate. If the gate is in the open state, then ion permeation should not be interrupted too often due to thermal fluctuations. This means that the value of R_2 in the open state has to be large enough so that $\Delta\Omega$ stabilizes the open gate. However, if R_2 is too large in the open state, which would cause the gate to be open constantly, the energy cost to close the gate would be too high. Similar arguments can be employed for the closed state. The closed state should also be stabilized against fluctuations, with sufficiently low energy costs. For our parameters, we can realize this situation if we assume that, for the open state, $R_2^{\mathrm{op}} \approx R_2^{\max} + 0.88R_{\mathrm{HS}} \approx R_2^{\max} + 1.23$ Å and $R_2^{\mathrm{cl}} \approx R_2^{\max} - 0.62R_{\mathrm{HS}} \approx R_2^{\max} - 0.87$ Å. In that case, the energy required to control the gate is roughly $5k_{\mathrm{B}}T$, which is comparable to the electrostatic energy gain of the voltage sensor of the potassium channel.

Finally, we can estimate ΔN, the number of liquid particles that leave the gate during a change in state in order to form the gas bubble. This is approximately related to the difference between the liquid density ρ_{l} and the gas density ρ_{g} and the volume of the bubble

$$\Delta N(R_2) \approx (\rho_{\mathrm{l}} - \rho_{\mathrm{g}})V(h_0, R_2 - R_{\mathrm{HS}}, R_{\mathrm{b}} - R_{\mathrm{HS}}), \tag{23}$$

where the volume $V(h_0, R_2 - R_{\mathrm{HS}}, R_{\mathrm{b}} - R_{\mathrm{HS}})$ is the volume that is accessible to the centres of fluid particles. For our system, we plot the result in figure 7. The quantity ΔN specifies the most likely number of particles that leave the gate. From this estimate, we conclude that roughly 17–24 fluid particles are involved in the transition between states. Since the bubble volume is rather small and the gas density is low, one is unlikely to find an appreciable amount of particles inside the bubble. Note that a more accurate estimate can be obtained from the thermodynamic relation

$$\Delta\tilde{N}(R_2) = -\left(\frac{\partial\Omega^{\mathrm{op}}_{\mathrm{gate}}(R_2) - \Omega^{\mathrm{cl}}_{\mathrm{gate}}(h_0, R_2)}{\partial\mu}\right)\bigg|_{T,V}. \tag{24}$$

The approximate expression, equation (23), takes only the volume term of the grand potentials into account and neglects the surface and curvature terms. In the present case, the estimate, equation (23), is sufficient to describe the properties of the bubble.

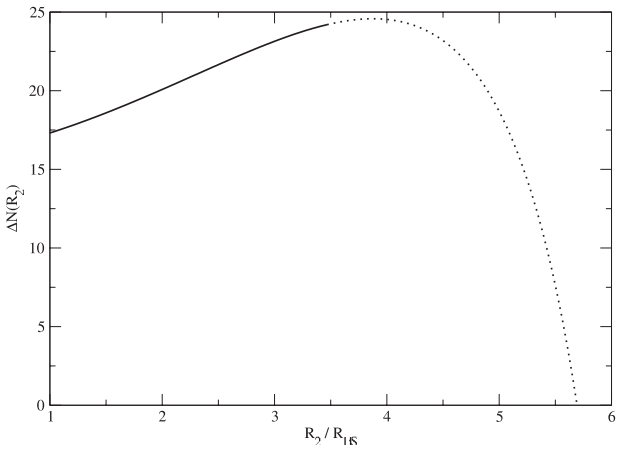

Figure 7. The number of fluid particles ΔN that leave the gate when a bubble forms to close the gate. If the gate is in the closed state, we plot ΔN as a full line; when the gate is open, we plot it as a dotted line.

5. Conclusion and outlook

We have presented a model for the opening and closing of a voltage-gated ion channel that follows the basic architecture of the potassium channel from Streptomyces lividans (KcsA) channel. The hydrophobically lined gate region changes from a wide pore, when open, to a narrower pore when closed. With our morphometric approach to capillary evaporation in a hydrophobic pore with cone-shaped geometry, we have shown that the formation of a bubble in the gate can close the permeation pathway of the channel and thereby stop the ion flux. When vapour forms in a channel, electric current cannot flow through the channel and the channel is *closed*. Ions cannot move into or through the vapour phase, and so the resistance to current flow is extremely large and the channel behaves like an *open*, i.e. disconnected, switch. The channel is closed to current flow in the biological sense of the word *closed*.

For the morphometric approach, we require a set of thermodynamic coefficients that we have determined in a simpler geometry within a set of DFT calculations for a square-well fluid. While the values of these coefficients differ significantly from the corresponding values for water, which is the fluid of biggest interest in the biological context of this model, a similar scenario should also be found in the case of water. It is the balance between different terms in the grand potential, i.e. the relative strength, rather than the absolute values of the thermodynamic coefficients that matters. Our model rationalizes recently seen bubble formation in computer simulations that employ more sophisticated models for water [14–23]. We thereby provide a basis for understanding the role of bubble formation and breaking in the gating process of voltage-gated ion channels on a deeper level. Since this model identifies the important physical driving forces of bubble formation, we hopefully provide a model that allows us to address, in addition to basic (unperturbed) gating, other important properties of ion channels, such as the effect of various chemicals that can change the environment in the gate, on the gating process.

In our study we have focused on the situation of changing geometry as a trigger for bubble formation. However, it is easy to see, within our description of a hydrophobic pore, that a second mechanism for bubble formation can be identified from the balance between the surface term $\Delta\sigma M$ and all the other terms in equation (22): if the geometry is kept constant, $\Delta\Omega$ can

still change sign and thereby favour the formation of a bubble if the degree of hydrophobicity and hence $\Delta\sigma$ is changed. This might be achieved if the gating process involves a change in fixed charges in the gate as a way of controlling the protein–fluid interaction.

A combination of geometrically controlled bubble formation, discussed in detail in this paper, and bubble formation due to a change in protein–fluid interaction, mentioned above, is of course also possible and might be of use in mechanosensitive ion channels such as the small mechanosensitive channel of Escherichia coli (MscS) channel [22].

Acknowledgments

RR is grateful to Wolfgang Nonner and Bob Eisenberg for many stimulating discussions about the role of bubble formation in the gating of ion channels and to Dirk Gillespie for comments on the manuscript.

References

[1] Burgess C G V, Everett D H and Nuttall S 1989 *Pure Appl. Chem.* **61** 1845
[2] Wong A P Y and Chan M H W 1990 *Phys. Rev. Lett.* **65** 2567
[3] Li J C, Ross D K and Benham M J 1991 *J. Appl. Crystallogr.* **24** 794
[4] Thommes M and Findenegg G H 1994 *Langmuir* **10** 4270
[5] Thommes M, Findenegg G H and Schoen M 1995 *Langmuir* **11** 2137
[6] Gross S and Findenegg G 1997 *Ber. Bunsenges. Phys. Chem.* **101** 1726
[7] Morishige K and Shikimi M 1998 *J. Chem. Phys.* **108** 7821
[8] Derjaguin B 1940 *Acta Physicocgimica URSS* **12** 181
[9] Evans R, Marconi U B M and Tarazona P 1986 *J. Chem. Soc., Faraday Trans.* 2 **86** 1763
[10] Evans R 1986 *J. Chem. Soc., Faraday Trans.* 2 **82** 1763
[11] Evans R 1990 *J. Phys.: Condens. Matter* **2** 8989
[12] Panagiotopoulos A Z 1987 *Mol. Phys.* **62** 701
[13] Gregg S J and Sing K S W 1967 *Adsorption, Surface Area, and Porosity* (London: Academic)
[14] Spohr E, Trokhymchuk A and Henderson D 1998 *J. Electroanal. Chem.* **450** 281
[15] Noworyta J P, Henderson D and Sokołowski S 1999 *Mol. Phys.* **96** 1139
[16] Allen R, Melchionna S and Hansen J P 2002 *Phys. Rev. Lett.* **89** 175502
[17] Allen R, Hansen J P and Melchionna S 2003 *J. Chem. Phys.* **119** 3905
[18] Dzubiella J and Hansen J P 2005 *J. Chem. Phys.* **122** 234706
[19] Beckstein O, Biggin P C and Sansom M S P 2001 *J. Phys. Chem.* B **105** 12902
[20] Beckstein O and Sansom M S P 2003 *Proc. Natl Acad. Sci. USA* **100** 7063
[21] Beckstein O and Sansom M S P 2004 *Phys. Biol.* **1** 42
[22] Anishkin A and Sukharev S 2004 *Biophys. J.* **86** 2883
[23] Sriraman S, Kevrekidis I G and Hummer G 2005 *Phys. Rev. Lett.* **95** 130603
[24] Hille B 2001 *Ion Channels of Exciteable Membranes* (Sunderland, MA: Sinauer Associates)
[25] See, e.g. Evans R 1992 *Fundamentals of Inhomogeneous Fluids* (New York: Dekker) p 85
[26] König P M, Roth R and Mecke K R 2004 *Phys. Rev. Lett.* **93** 160601
[27] Roth R 2005 *J. Phys.: Condens. Matter* **17** S3463
[28] Parry A O and Evans R 1992 *J. Phys. A: Math. Gen.* **25** 275
[29] Roth R, Evans R, Lang A and Kahl G 2002 *J. Phys.: Condens. Matter* **14** 12063
[30] Yu Y-X and Wu J 2002 *J. Chem. Phys.* **117** 10156
[31] Rosenfeld Y 1989 *Phys. Rev. Lett.* **63** 980
[32] Sullivan D E, Levesque D and Weiss J J 1980 *J. Chem. Phys.* **72** 1170
[33] Bryk P, Roth R, Mecke K R and Dietrich S 2003 *Phys. Rev.* E **68** 031602
[34] Roth R and Gillespie D 2005 *Phys. Rev. Lett.* **95** 247801
[35] Ustinow E A and Do D D 2005 *Adsorption* **11** 455
[36] Doyle D A *et al* 1998 *Science* **280** 69
[37] Jiang Y *et al* 2002 *Nature* **417** 515